NASA-TM-84235 19820021279

# BRDF Measurements of Sunshield and Baffle Materials for the IRAS Telescope

Sheldon M. Smith

May 1982



NASA
National Aeronautics and
Space Administration

NASA Technical Memorandum 84235

# BRDF Measurements of Sunshield and Baffle Materials for the IRAS Telescope

Sheldon M. Smith, Ames Research Center, Moffett Field, California

NASA
National Aeronautics and
Space Administration

**Ames Research Center**
Moffett Field, California 94035

# BRDF MEASUREMENTS OF SUNSHIELD AND BAFFLE MATERIALS FOR THE IRAS TELESCOPE

Sheldon M. Smith

Ames Research Center

## SUMMARY

Measurements of the far-infrared bidirectional reflectance distribution functions (BRDF) of four samples of Martin Black coating and one sample of gold coated aluminum from the telescope to be flown on the Infrared Astronomy Satellite (IRAS) are presented. At incidence angles near 35°, Martin Black is a diffuse reflector at wavelengths as long as 36 μm. The gold coated aluminum sample from the IRAS sunshield has a visible grain which causes a strong diffraction enhancement of the BRDF at large nonspecular angles. This enhancement from the sunshield will increase the stray light level inside the telescope.

## INTRODUCTION

A nonspecular reflectometer (NSR), recently constructed at Ames Research Center in support of the Shuttle Infrared Telescope Facility (SIRTF), was used to measure the bidirectional reflectance distribution function (BRDF) of four light baffles coated with Martin Black and one sample of sunshade material from the telescope of the Infrared Astronomy Satellite (IRAS). Stray light rejection is very important in the design and operation of space telescopes such as SIRTF, IRAS, and COBE (Cosmic Background Explorer), because they must often point toward astronomical objects whose direction is not far from that of bright, extended sources. Knowledge of the BRDF of certain critical surfaces is required to calculate the amount of stray light reaching the telescope focal plane and to thus evaluate off-axis rejection characteristics. The samples and angles described here were selected by the IRAS Project and are specific to the IRAS telescope; however, their far-infrared reflectance characteristics are similar to those of several other optical black coatings that have been measured. The sunshield material performs as a surprisingly good infrared reflection grating.

## INSTRUMENTATION

Although the NSR has been described before (ref. 1), it will be briefly described again to define terms and angles. The instrument is a far-infrared goniometer-photometer utilizing bandpass transmission filters (ref. 2) with spectral resolutions between 3% and 22%. Additional short-wave blocking is provided by a long-wave pass interference filter designed by Whitcomb and Keene (ref. 3). The major components of the NSR are shown in figure 1 where, for convenience, the detector (a Ga:Ge bolometer) has been shown to rotate. The angle of reflection or scattering $\theta_s$ is continuously variable between ±10° and ±90°. When a gold coated mirror replaces the black substrate, the aperture of the blackbody source is

specularly imaged inside the detector's field stop by an f/33 ellipsoid of revolution when the nonspecular angle $\Delta\theta$ is zero, that is, when the detector is located so that the angle of incidence $\theta_i$ equals the angle of reflection. From Figure 1, then,

$$\Delta\theta = \theta_s - \theta_i \tag{1}$$

The projection of $\Delta\theta$ onto the plane of the substrate is $\Delta\beta$, and can be seen from the figure to be

$$\Delta\beta = \sin\theta_s - \sin\theta_i \tag{2}$$

In backward scattering both $\Delta\theta$ and $\Delta\beta$ are negative, which is usually indicated on BRDF plots by labels rather than signs.

The BRDF is the reflectance per unit projected solid angle. Since the detector subtends a solid angle $\omega_d$ of only $9\times10^{-4}$ sr ($d\theta = 1.94°$), the NSR is highly directional. The reflectance $R$ is obtained from the ratio of reflected to incident power measured through the same bandpass filter at wavelength $\lambda$:

$$R(\lambda,\theta_s,\theta_i) = \frac{V_{sb}(\lambda,\theta_s,\theta_i)}{V_g(\lambda,\theta_i)} \tag{3}$$

where $V_{sb}$ refers to the reflected power scattered by a black coating into the detector located at some angle $\theta_s$, and $V_g$ refers to the incident power reflected by a gold coated glass mirror into the detector when it is located at the specular angle. From the definition of BRDF (ref. 4), then,

$$BRDF(\lambda,\theta_s,\theta_i) = \frac{R(\lambda,\theta_s,\theta_i)}{\omega_d \cos\theta_s} \tag{4}$$

The angle of incidence $\theta_i$ is, of course, a constant during any BRDF measurement so that $R$ and BRDF are often plotted as functions of $\Delta\theta$ or $\Delta\beta$. However, the reflectance of rough surfaces depends strongly on $\theta_i$, so it must be clearly indicated on such plots. Only certain "well-behaved" surfaces whose surface roughness is much smaller than the wavelength are not dependent on incidence angle (ref. 5).

The beam shape or instrument profile (IP) of the NSR is given by the relative reflectance of gold coated glass [replace $V_{sb}(\lambda,\theta_s,\theta_i)$ by $V_g(\lambda,\theta_s,\theta_i)$ in equation (3)]. It is directly related to wavelength and inversely related to the diameter of the ellipsoidal bending mirror; hence, it is presumed to be principally caused by $\lambda/d$ diffraction. Because the angular width of the IP increases with wavelength, nonspecular reflectance measurements of optical black coatings must be corrected for their contribution to measured signals. The correct way to do this is to deconvolve the IP from the true reflectance by means of Fourier analysis. However, such analysis requires a great deal more experimental data than are presently available. In the absence of those data, an approximate correction will be attempted on the assumption that black coatings become as specularly reflecting at far-infrared wavelengths as gold coated glass. This correction is then accomplished by

$$\underset{\text{corrected black}}{\text{BRDF}(\lambda,\Delta\theta)} = \underset{\text{measured black}}{\text{BRDF}(\lambda,\Delta\theta)} - \underset{\text{measured black}}{R(\lambda,\Delta\theta = 0)} \; \underset{\text{gold coated glass}}{\text{BRDF}(\lambda,\Delta\theta)} \tag{5}$$

The correcting term increases with wavelength, becoming as large at $\Delta\theta = 3°$ as 75% at 234 μm on sample I1-1. It is also inversely related to $\Delta\theta$ since the BRDF of gold coated glass is a very steep function.

Vertical error bars at the left side in each of figures 2 through 8 indicate the total absolute error in the BRDF measured at small values of $\Delta\theta$. The errors result from random error propagation among the principal uncertainties of variable humidity, detector response, and substrate alignment. The measurements proceed from the specular angle (usually in 1° increments of $\Delta\theta$) until the signal falls below the noise level. Thus, at the end of a data sequence the error may be somewhat larger than shown. The data point at $\Delta\theta = 2°$ is most susceptible to alignment error and is included in the figures only because of the scarcity of long-wavelength data. Unfortunately, the correction for instrument profile described above nearly doubles the total error. Horizontal error bars are unnecessary since $\theta_s$ and $\theta_i$ are read to better than 1°.

## Reflectance of IRAS Baffle Materials

The samples described below were measured specifically for the IRAS project and so do not provide a thorough study of the reflectance of the Martin Black coating. However, the measurements can be taken as representative of Martin Black at the angles indicated. One sample (I1-1) is being studied further at the University of Arizona to fill in gaps left by this survey (W. F. Wolfe, personal communication).

The first two samples demonstrate reflectance properties that have been found to be characteristic of several other optical black coatings in the far-infrared. In figures 2 and 3 one can see that not only does the reflectance level increase with wavelength, but the slope of the BRDF increases with wavelength also. The lower curves, at 36 μm, are flat and nearly horizontal, indicating a very diffuse reflectance. (A Lambertian surface has a horizontal BRDF.) By 110 μm the slope is greatly increased, and at 234 μm the measured BRDF approaches the instrument profile shown by the dashed lines in figure 3. This behavior indicates that as wavelength increases the surface becomes <u>both</u> smooth and nonabsorbing.

Although figures 2 and 3 present the forward and backward scatter of two different samples of Martin Black, there is no obvious difference in the measurements at 36 μm. Larger differences between the measurements at the longer wavelengths are probably more an indication of low signal-to-noise ratio than of sample difference.

The IRAS project required that the next pair of samples of Martin Black coated baffle material be measured at a very large angle of incidence (75°). To accommodate this large angle, the ellipsoidal bending mirror was stopped down in one dimension so that the incident source beam did not project over the edge of the sample. The narrow stop also broadened the instrument profile. At this large angle of incidence the specular reflectance was so large (~50%) that equation (5) often produced a negative result, hence these data were not corrected for instrument profile. Instead, the instrument profile is shown by dashed curves in figure 4 next to the uncorrected measurements. These data are also restricted to nonspecular angles less than 6°

because at larger angles the detector begins to see the source directly, without reflection off the sample.

Inspection of figure 4 indicates that these two samples have very similar glancing-angle reflectances. Direct comparison with figures 2 and 3 is not possible because of the different instrument profiles. However, it should be noted that the change in the 36 μm BRDF from 35° to 75° incidence far exceeds the difference in instrument profile. Dependence on incidence angle is a characteristic of a rough surface, and it has been noted before (ref. 1) that Martin Black demonstrates such a dependence at 36 μm. The very large increase in 36 μm slope just noted indicates that the coating becomes effectively smooth at 75° incidence.

## IRAS Sunshield Material

This study of the IRAS sunshield has provided an interesting application of diffraction grating theory. The sunshield material is rolled aluminum that has been coated with gold. Unfortunately, the gold coating does not cover up a visually apparent pattern of parallel scratches or grooves which is most probably related to the rolling process.

In figure 5 the 12 μm BRDFs of this material, when the sample is oriented at three different elevation angles with respect to the source-detector plane, are compared with the instrument profile (gold coated glass). At $\Delta\beta > 0.08$, the sunshield data show structure that is related to the orientation of the sample. At large $\Delta\beta$ the reflectance is strongly enhanced above the instrument profile at each of the three orientations. In particular, it should be noted that the greatest BRDF occurs when the sunshield is oriented vertically, that is, with the grain of the material perpendicular to the source-detector plane in the correct orientation for a diffraction grating. The hump in the horizontal data near $\Delta\beta = 0.2$ is quite unusual and may possibly be related to a small curvature of the sample.

In both figures 6 and 7 the sample is oriented perpendicular to the source-detector plane (i.e., vertically), but at two different angles of incidence. BRDFs at two wavelengths are shown, and the instrument profile at 12 μm is given for comparison. Vertical arrows point toward inflection points in the IRAS data near $\Delta\beta = 0.1$. Note that this inflection moves to larger $\Delta\beta$ with increasing wavelength. At 12 μm, a third inflection point can be seen in each figure near $\Delta\beta = 0.9$. Note that this large-angle inflection has the opposite sense to that at small $\Delta\beta$. In figure 7 the range where data were not available at 15° incidence, because the source and detector would have been superimposed, is indicated by a dashed line. Observe that the large-angle inflection occurs at the extrapolation of the preceding seven available data points, and figure 5 clearly shows that both the large- and small-angle inflection points are connected by a smooth, continuous signal.

The facts just noted can be completely explained by the thesis that the usual instrument profile given by a smooth glass surface has been enhanced by diffraction from an unusual grating whose groove spacing has a continuous variation or distribution. The well known equation of the diffraction grating (ref. 6) can be written in terms of $\Delta\beta$ by use of equation (2),

$$m\lambda = d\,\Delta\beta\,, \qquad m = \pm 1, \pm 2, \ldots \tag{6}$$

where $d$ is the grating space and $m$ is the order of interference. Given a conventional grating and a discrete wavelength, a series of discrete lines will occur in $\Delta\beta$ space corresponding to increasing values of $m$. When a continuous spectrum illuminates the grating, the region between the discrete lines of adjacent orders fills in with diffracted light of the proper wavelength. The case at hand is inversely analogous to the continuous spectrum: instead of all wavelengths being present and only one spacing, a continuum of grating spaces is available to one well-defined wavelength. The result is the same, the region in $\Delta\beta$ space between adjacent orders fills in continuously with light diffracted from the proper groove spacing.

At the bottom of figure 6, the uppermost set of lines shown corresponds to the conventional case of increasing orders from a discrete grating space (148 μm) and wavelength (12.25 μm). The width of these lines is proportional to the effective width of the filter passband. Directly beneath them are lines corresponding to the inverse analogy for a specific order (first, the strongest) and a fixed wavelength. In the conventional case, $\Delta\beta$ increases with the order; in the inverse case $\Delta\beta$ increases with decreasing grating space. According to the above thesis, the large-angle inflection signifies the end of the 12 μm diffraction enhancement. It can be seen that it occurs at the smallest grating space. Evidently, the enhancement ceases because smaller spacings are not available. Using the effective filter wavelength of 12.25 μm, $m = 1$, and $\Delta\beta = 0.660$ from figure 6, equation (6) produces $d_{min} = 18.5$ μm. This is an accurate measurement because the bandpass of the 12 μm filter is only 3% of the wavelength corresponding to $\Delta\beta$, and the ~2% subtense of the detector is less than the separation of the data points at this end of the spectrum. The similar large-angle enhancement in figure 7 produces a value of $d_{min} = 15.7$ μm after an instrument-related dependence on $\theta_i$ is cancelled out by superposition of instrument profiles. These two measurements differ by only 16% and are in good agreement with a scanning electron microscope inspection of the sunshield material, which indicated that the smallest spacing is between 10 μm and 20 μm.

The small-angle inflections occur at the low resolution end of the spectrum corresponding to large grating spaces. The resolution is low here because not only does the detector subtense span nearly three data points, but the separation between adjacent orders is shrinking. Thus, the data point under the 12 μm arrow in figure 6 may include as many as four of the analogous orders. This low resolution overlap of orders explains why the intensity of the enhancement increases at small $\Delta\beta$. Although increasingly large spacings are undoubtedly available on the sample, the very steep instrument profile eventually overpowers the diffraction enhancement creating the small-angle inflection in the BRDF. At 12 μm, this occurs at $\Delta\beta < 0.07$ and $d \gtrsim 200$ μm.

At 36 μm the small-angle inflection moves to larger values of $\Delta\beta$ in accordance with equation (6). The much larger spectral width of the 36 μm filter is indicated by broader lines at the bottom of figure 6 where the overlap of orders can be seen to commence much sooner. Light diffracted by the smallest spacing (18 μm) lies at $\Delta\beta \approx 2$, and is below the noise level of the NSR. In spite of the decrease in resolution, some quantitative information may still be garnered from the small-angle inflections. The change in $\Delta\beta$ with wavelength, or $\delta(\Delta\beta)$, shown by the arrows in figures 6 and 7, can be evaluated from the total derivative of equation (6):

$$\delta\lambda = d\delta(\Delta\beta) + (\Delta\beta)\delta d \qquad (7)$$

Evaluating this at 12 μm, using $\delta(\Delta\beta)$ from both figures 6 and 7, gives the change in grating space with wavelength $\delta d = 221$ μm. Thus, equation (7) predicts that at 36 μm the small-angle inflection point will indicate a grating space of

221 + 148 = 369 μm. Inserting this value into equation (6) with $m\lambda = 36$ μm gives $\Delta\beta$ at 36 μm of $9.8\times10^{-2}$. This differs from the value of $\Delta\beta$ read directly below the arrow in figure 6 by less than 12%.

A final point about the data may be noted. The enhancements shown in figures 6 and 7 are identical, although the inflection points do not appear to fall at the same values of $\Delta\beta$. This apparent dependence on $\theta_i$ is a property of the 12 μm instrument profile and not of the diffraction enhancement. When figures 6 and 7 are shifted in $\Delta\beta$ to superimpose the instrument profiles, as shown in figure 8 at 12 μm, the enhancements then appear identical. The scale at 35° incidence (fig. 6) is considered the most accurate and has been used exclusively in the above calculations. It is convincing that the observed diffraction enhancements are independent of $\theta_i$ as indicated by equation (6).

In conclusion, the large-angle nonspecular reflectance of the IRAS sunshield material is enhanced at least two orders of magnitude above that of a smooth surface by diffraction from a continuous distribution of parallel grooves. The enhancement at a wavelength of 12 μm extends to a nonspecular angle of 40° and ceases beyond that angle because grating spaces smaller than about 18 μm are not present. At longer wavelengths the enhancement will extend to larger angles in accordance with the grating equation. Since the telescope aperture lies at nonspecular angles of 45° and larger, it will be contaminated with long wavelength sunlight diffracted by the grooves on the sunshield.

## ACKNOWLEDGMENTS

The author would like to acknowledge constructive discussions regarding the diffraction grating with Stuart Bowen and Francisco Valero, both of Ames Research Center. The scanning electron microscope inspection was done by Homer Lem of E.A.L. Corp., Richmond, CA.

## REFERENCES


1. Smith, S. M.: Far-Infrared (FIR) Optical Black Bidirectional Reflectance Distribution Function (BRDF). SPIE, vol. 257, 1981, p. 161.

2. Sakai, K.; and Yoshida, T.: Single Mesh Narrow Bandpass Filters from the Infrared to the Submillimeter Region. Infrared Phys., vol. 18, 1978, p. 137.

3. Whitcomb, S. E.; and Keene, J.: Low-Pass Interference Filters for Submillimeter Astronomy. Appl. Opt., vol. 19, 1980, p. 185.

4. Nicodemus, F. E.: Directional Reflectance and Emissivity of an Opaque Surface. Appl. Opt., vol. 4, 1965, p. 767.

5. Harvey, J. E.: Light-Scattering Characteristics of Optical Surfaces. Ph.D. Thesis, U. of Arizona, 1976.

6. Born, M.; and Wolf, E.: Principles of Optics. Pergamon Press, 4th Ed., 1970, p. 403.

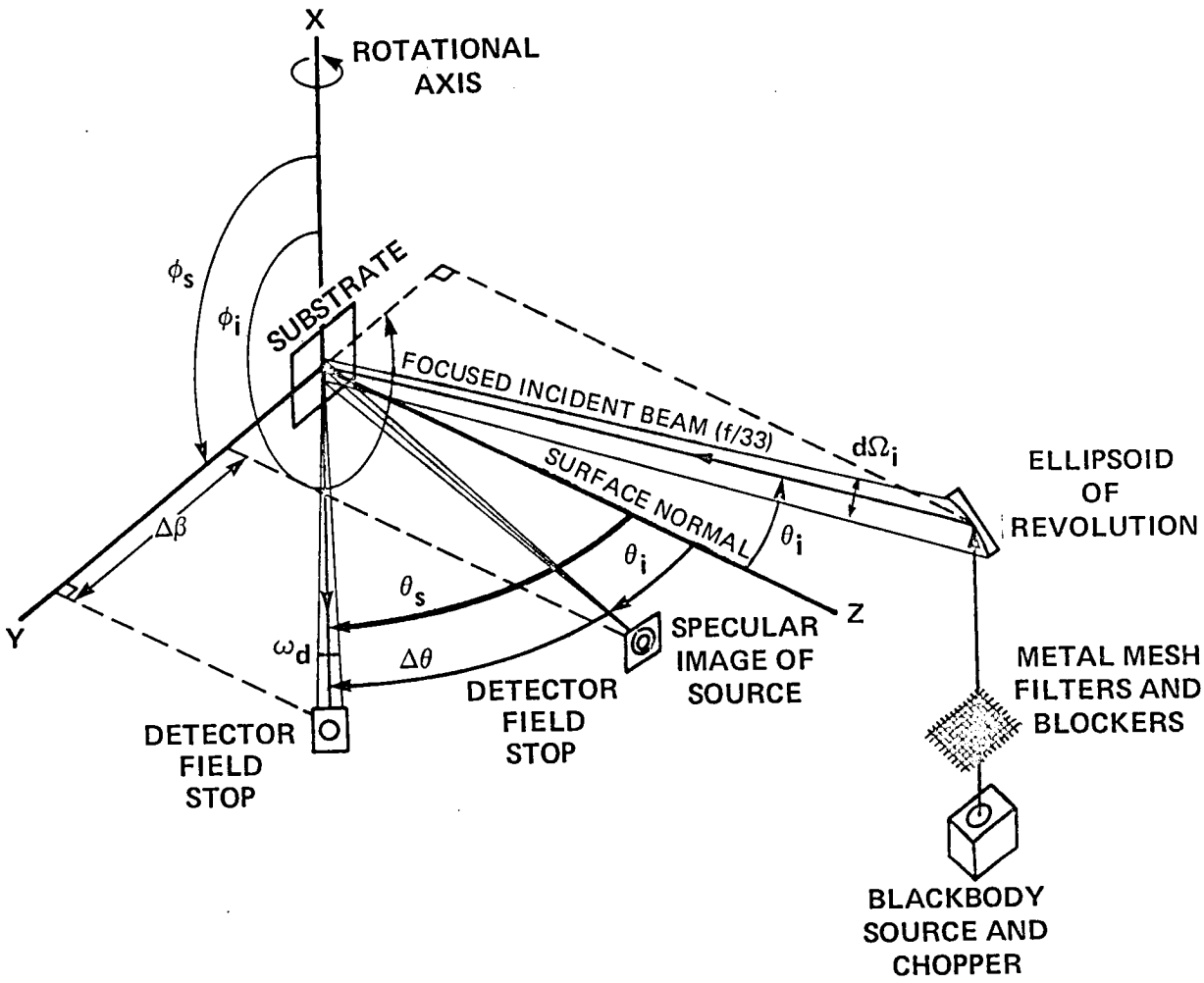


Figure 1. Schematic drawing of the nonspecular reflectometer.

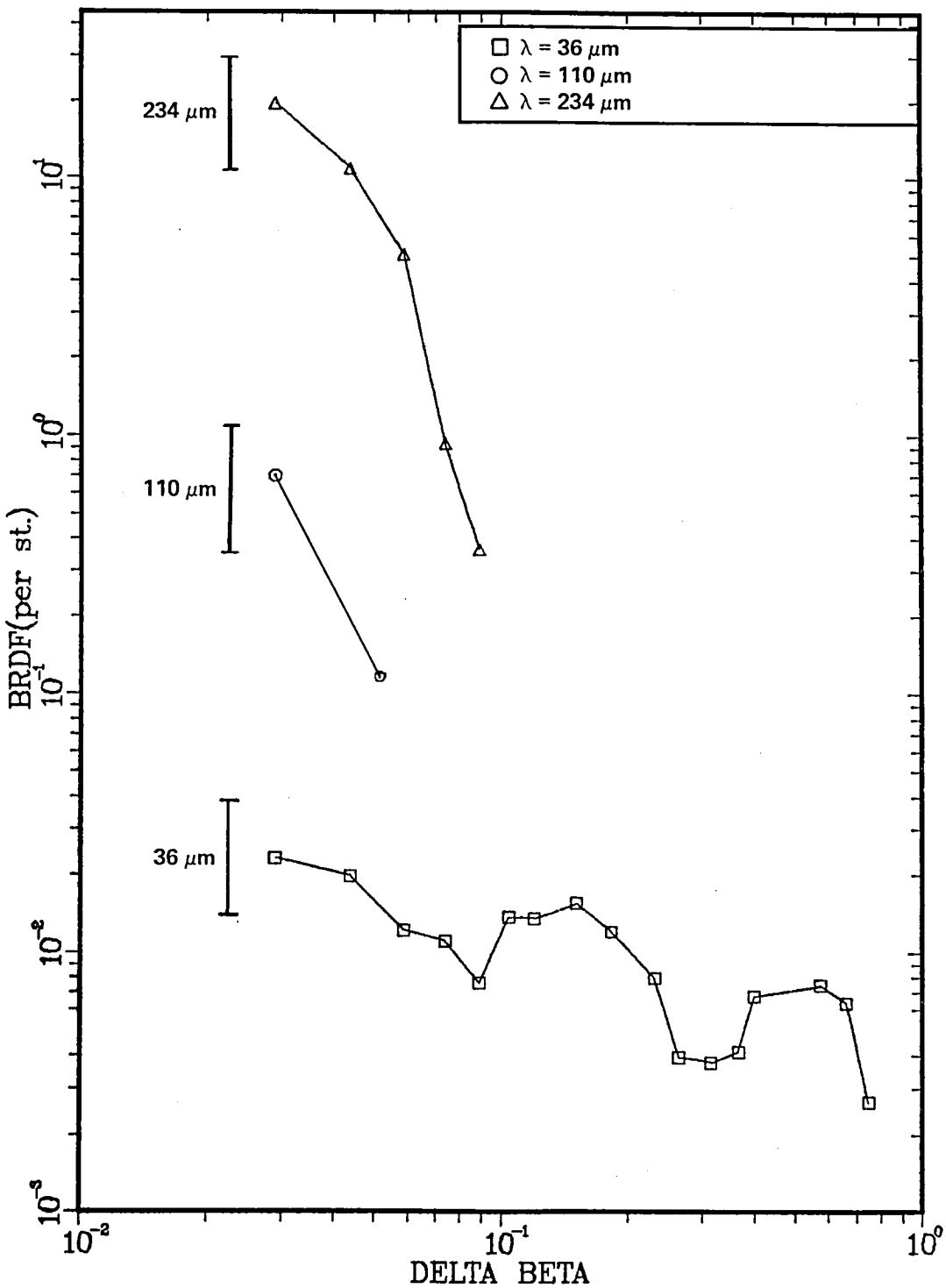


Figure 2. BRDF measurements of IRAS sample G1-1 at three far-infrared wavelengths. Vertical error bars refer to the total error.

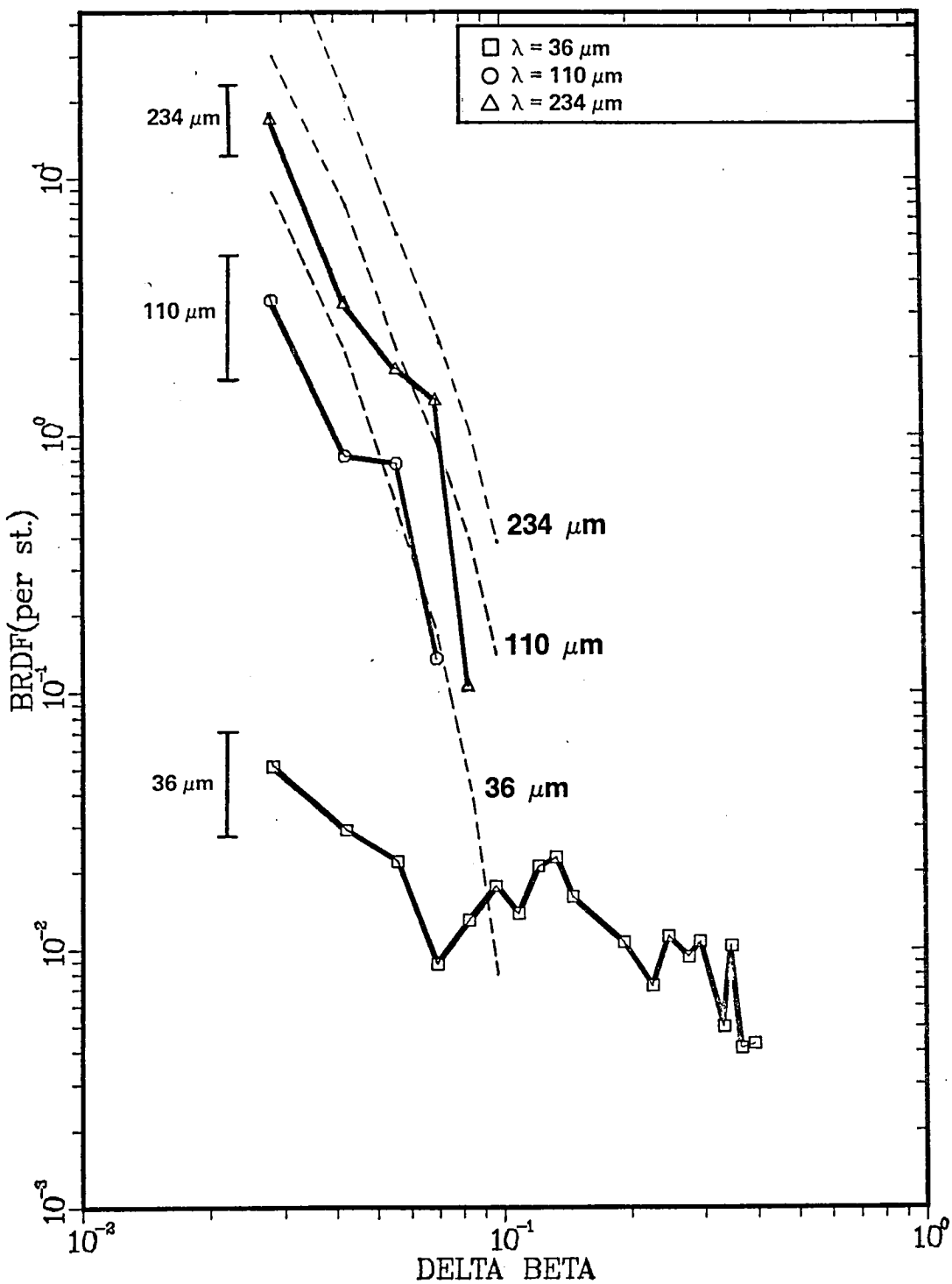


Figure 3. BRDF measurements of IRAS sample I1-1 at three far-infrared wavelengths. Instrument profiles at those wavelengths are indicated by dashed lines. Vertical error bars refer to the total error.

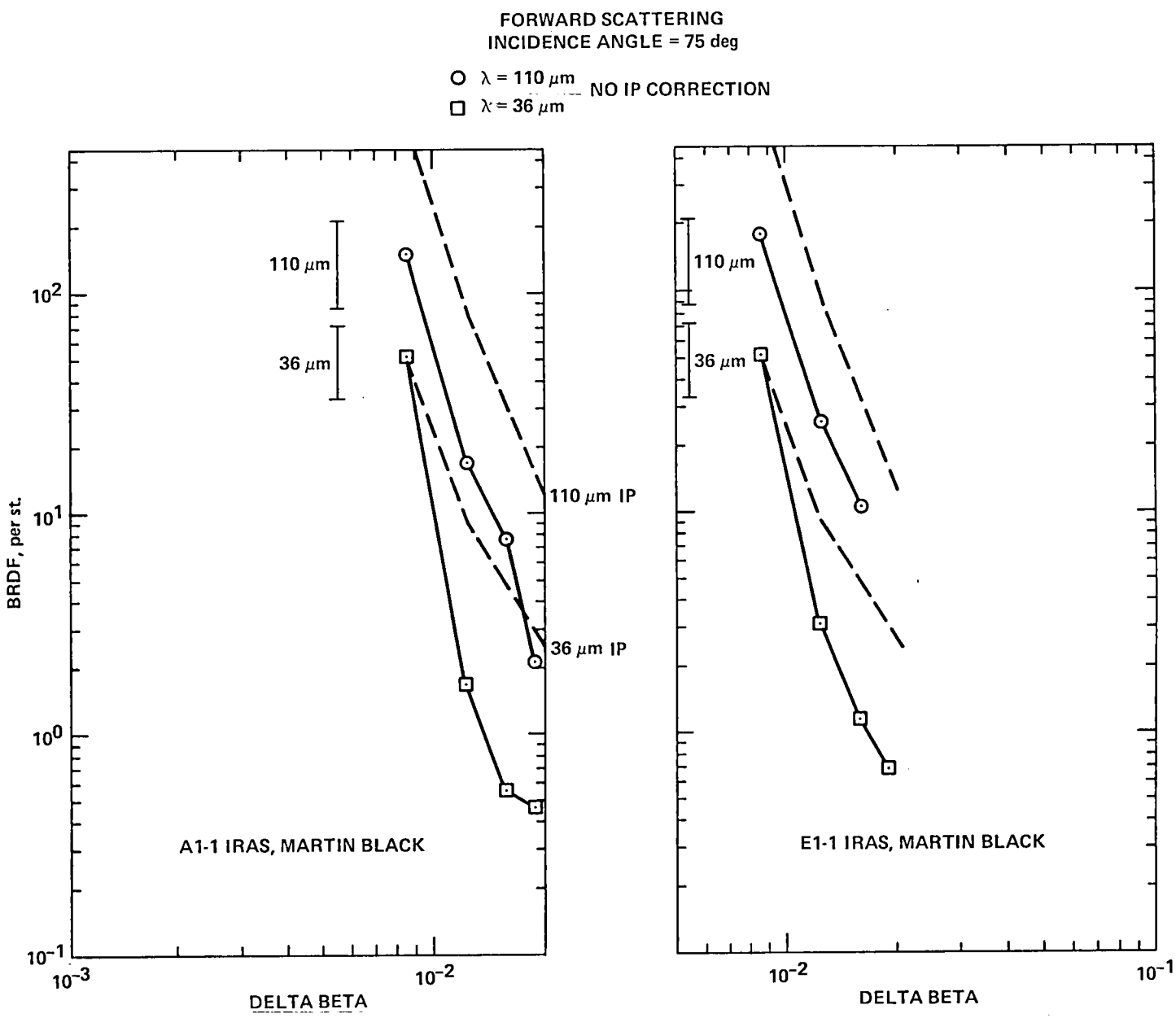


Figure 4. Glancing incidence BRDF measurements of two IRAS samples at two wavelengths. Instrument profiles at 36μm and 110 μm are indicated by dashed lines. Vertical error bars refer to the total error of a single measurement.

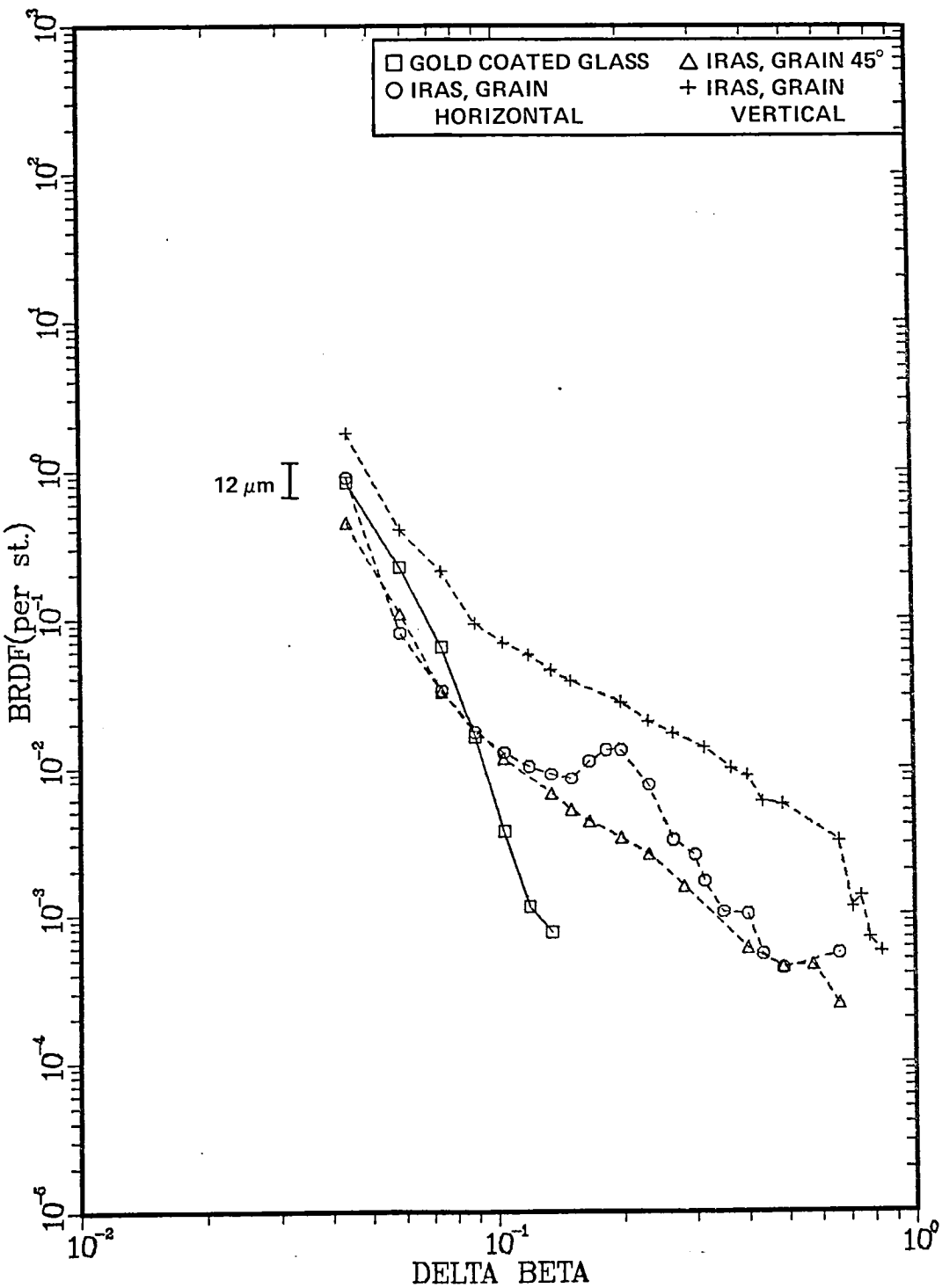


Figure 5. BRDF measurements of IRAS sunshield material at 12 μm wavelength. The sample was oriented at three different angles to the source-detector plane, which was horizontal. The instrument profile is indicated by a solid line and the error bar refers to the total error. Note that there are two inflections of opposite sense in the curve for the vertical orientation.

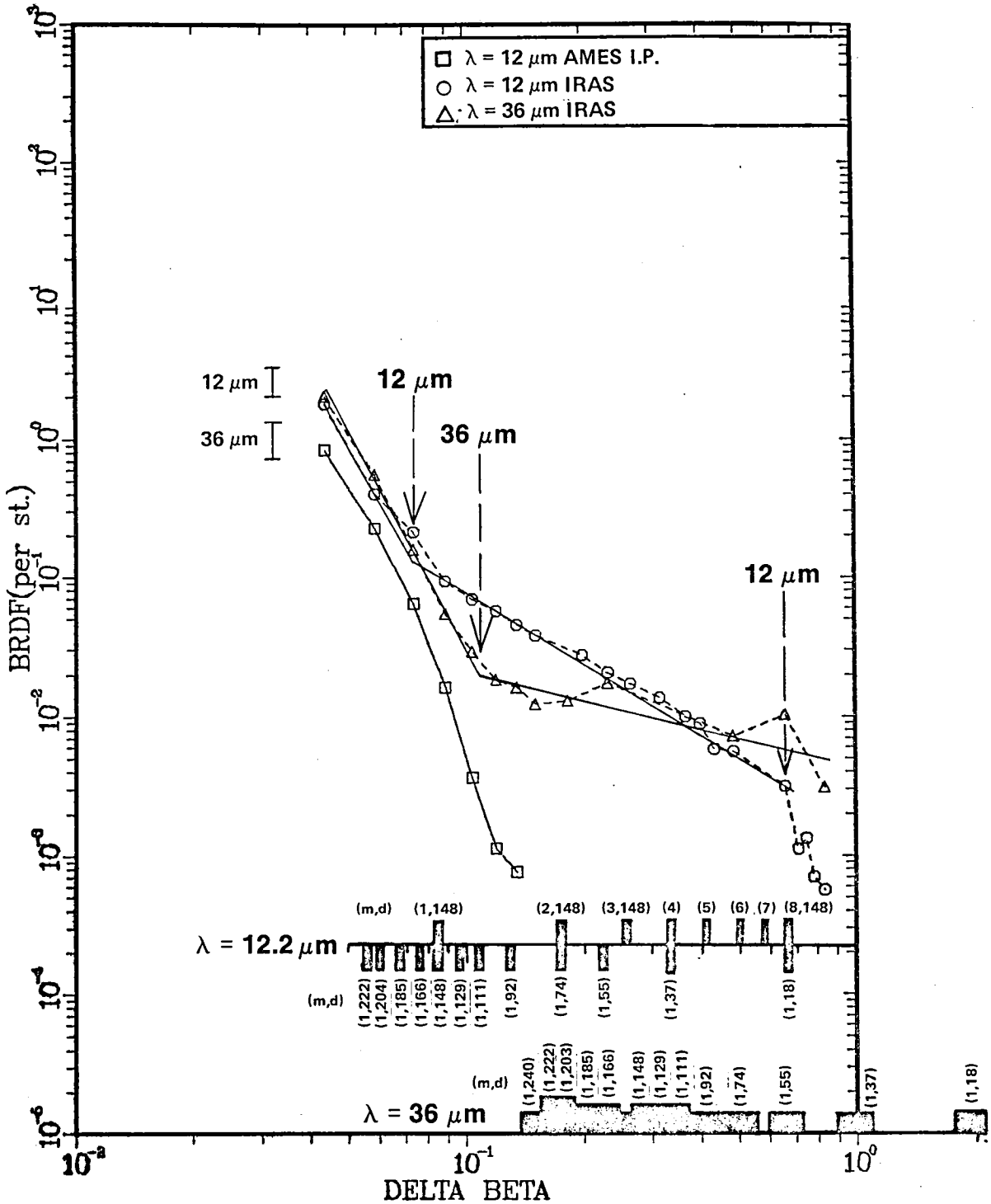


Figure 6. Vertically oriented sample at 35° incidence: BRDF measurements at two wavelengths. The 12 μm instrument profile is indicated by the solid line and the error bars refer to total error. Inflection points are located by vertical arrows. Below the curves are three sets of lines indicating the location of different orders of diffraction and different grating spaces.

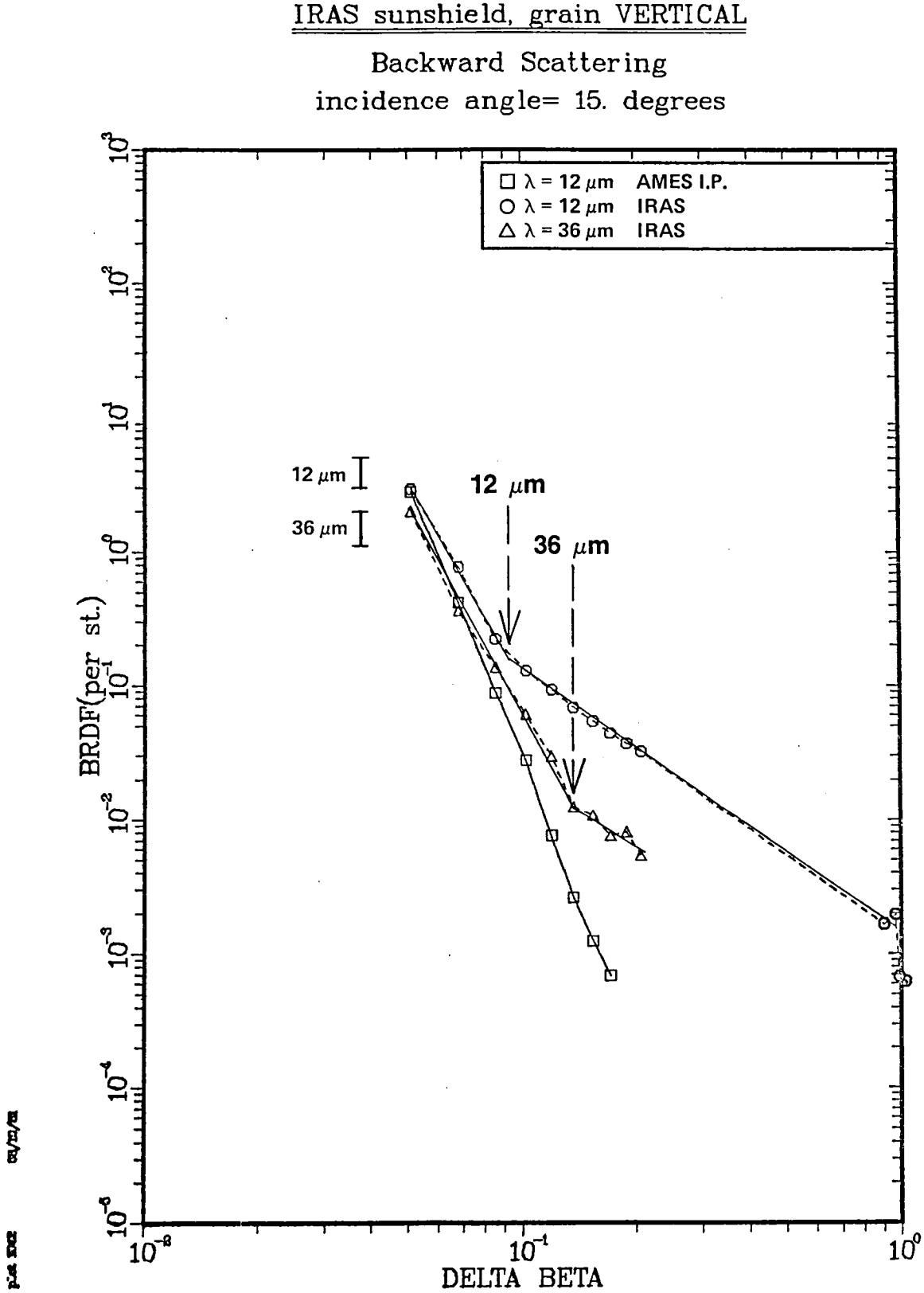


Figure 7. Vertically oriented sample at 15° incidence: BRDF measurements at two wavelengths. The 12 μm instrument profile is indicated by the solid line and the error bars refer to total error. Note the four data points at the right edge of the figure which comprise the large angle inflection. Vertical arrows locate the two small angle inflection points.

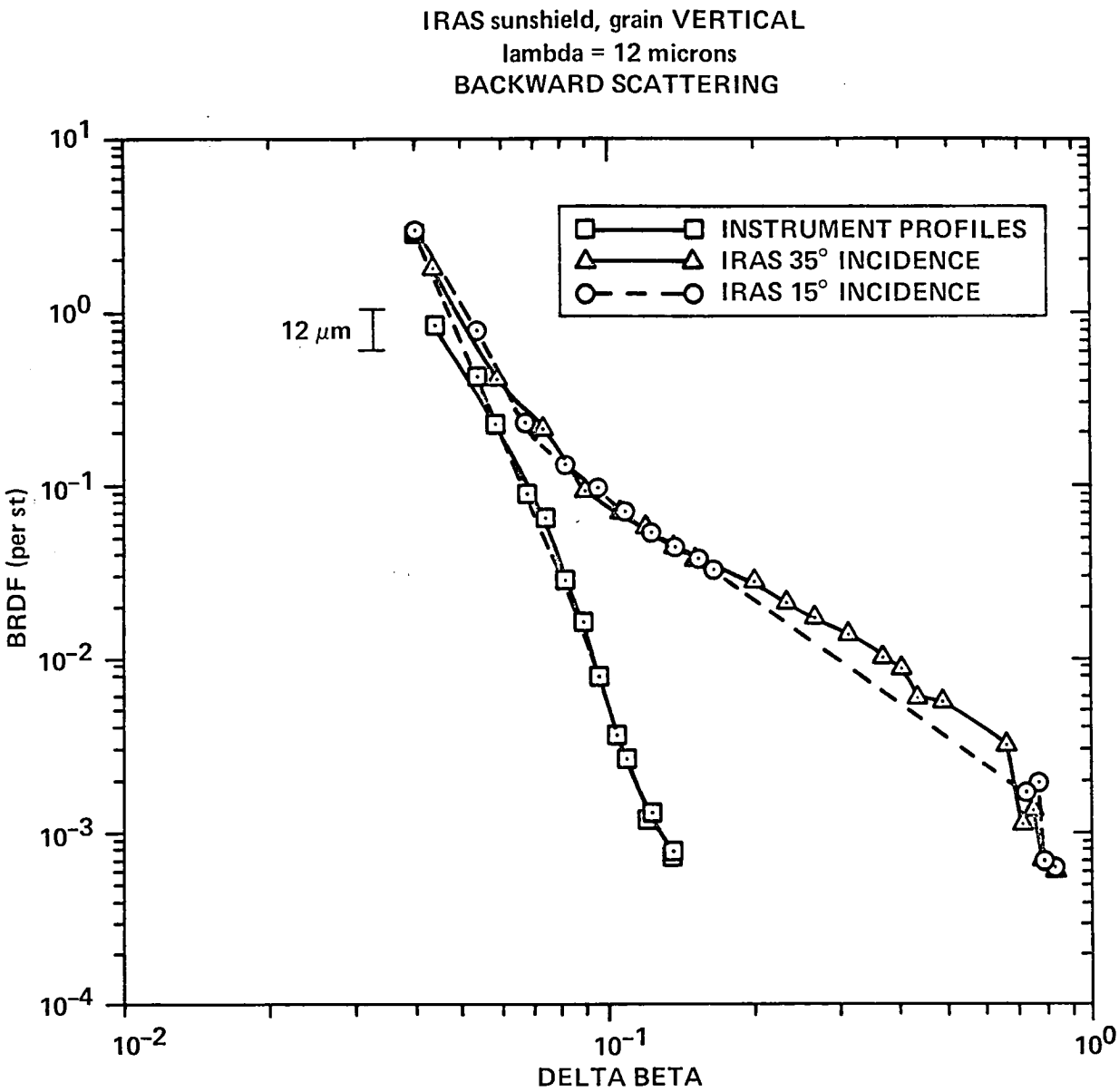


Figure 8. Diffraction enhancements at two different angles of incidence, $\lambda$ = 12 μm. The 12 μm instrument profiles have been super imposed by a shift in $\Delta\beta$ to cancel an instrument related dependence on $\theta_i$. The abscissae are the same as at 35° incidence.

| 1. Report No. | 2. Government Accession No. | 3. Recipient's Catalog No. |
|---|---|---|
| NASA TM-84235 | | |

| 4. Title and Subtitle | 5. Report Date |
|---|---|
| BRDF MEASUREMENTS OF SUNSHIELD AND BAFFLE MATERIALS FOR THE IRAS TELESCOPE | June 1982 |
| | 6. Performing Organization Code |
| 7. Author(s) | 8. Performing Organization Report No. |
| Sheldon M. Smith | A-8887 |
| | 10. Work Unit No. |
| 9. Performing Organization Name and Address | T-5196 |
| NASA Ames Research Center<br>Moffett Field, CA 94035 | 11. Contract or Grant No. |
| | 13. Type of Report and Period Covered |
| 12. Sponsoring Agency Name and Address | Technical Memorandum |
| National Aeronautics and Space Administration<br>Washington, D.C. 20546 | 14. Sponsoring Agency Code<br>159-41-06-02 |

15. Supplementary Notes

Point of Contact: Sheldon M. Smith, MS 245-6,
NASA Ames Research Center, Moffett Field, CA. 94035
FTS 448-6264 or (415) 965-6264

16. Abstract

Measurements of the far-infrared bidirectional reflectance distribution functions (BRDF) of four samples of Martin Black coating and one sample of gold coated aluminum from the telescope to be flown on the Infrared Astronomy Satellite (IRAS) are presented. At incidence angles near 35°, Martin Black is a diffuse reflector at wavelengths as long as 36 μm. The gold coated aluminum sample from the IRAS sunshield has a visible grain which causes a strong diffraction enhancement of the BRDF at large nonspecular angles. This enhancement from the sunshield will increase the stray light level inside the telescope.

| 17. Key Words (Suggested by Author(s)) | 18. Distribution Statement |
|---|---|
| BRDF<br>Telescope sunshield<br>Telescope baffle coating<br>Infrared | Unlimited<br><br>Subject Category - 74 |

| 19. Security Classif. (of this report) | 20. Security Classif. (of this page) | 21. No. of Pages | 22. Price* |
|---|---|---|---|
| Unclassified | Unclassified | 18 | A02 |

*For sale by the National Technical Information Service, Springfield, Virginia 22161